N O T I C E

THIS DOCUMENT HAS BEEN REPRODUCED FROM MICROFICHE. ALTHOUGH IT IS RECOGNIZED THAT CERTAIN PORTIONS ARE ILLEGIBLE, IT IS BEING RELEASED IN THE INTEREST OF MAKING AVAILABLE AS MUCH INFORMATION AS POSSIBLE

(NASA-TM-82103) CALIBRATION OF A GAMMA-RAY TELESCOPE USING TAGGED POSITION ANNIHILATION PHOTONS (NASA) 25 p HC A02/MF A01 CSCL 03B

N81-20002

Unclas

G3/93 19347

NASA

Technical Memorandum 82103

Calibration of a Gamma-Ray Telescope Using Tagged Positron Annihilation Protons

D.L.Bertsch and W.R.Dodge

FEBRUARY 1981

APR 1981
RECEIVED
NASA STI FACILITY
ACCESS DEPT.

National Aeronautics and
Space Administration

Goddard Space Flight Center
Greenbelt, Maryland 20771

CALIBRATION OF A GAMMA-RAY TELESCOPE USING TAGGED POSITRON ANNIHILATION PHOTONS

D. L. Bertsch
Goddard Space Flight Center
Greenbelt, Maryland 20771, U.S.A.

W.R. Dodge
National Bureau of Standards
Washington, DC 20234, U.S.A.

ABSTRACT

Measurements of detection efficiency, angular resolution, and energy resolution properties of a gamma-ray telescope used to study celestial gamma rays from balloon-flight altitudes are described. Nearly monochromatic photons produced at the National Bureau of Standards tagged-photon facility were used for the calibration. Details of the photon beam configuration and properties and results of the measurements made at photon energies of 15.1 and 31.1 MeV are presented. Finally, the data are compared with a Monte Carlo analysis of the instrument properties.

1. INTRODUCTION

The determination of the absolute detection efficiency, angular, and energy resolution of gamma-ray telescopes has long been a difficult and uncertain process because of the lack of suitable sources of high energy monochromatic photons. Analytic calculations provide a valuable guide for understanding a telescope's behavior; however, a check of such evaluations by direct measurements is highly desireable since the complexity of the instruments and the large variety of possible types of interaction histories that must be considered in any analysis requires many simplifying approximations whose cummulative effect is always somewhat uncertain.

Among the various processes that are available for producing gamma rays suitable for calibration of most gamma-ray telescopes designed for astronomical studies, only electron bremsstrahlung and positron annihilation are capable of yielding photons from 10 MeV to substantially higher energies. Tagged bremsstrahlung beams were used to calibrate the OSO-3 high energy detector[1], and the SAS-2[2,3], and COS-B[4,5] gamma-ray telescopes. The main difficulties with this approach were the relatively large energy dispersion at lower energies and the small fraction of the total incident bremsstrahlung beam in the appropriate energy interval for tagging. For example, the calibration beam for COS-B[5] had a FWHM dispersion of $\Delta E/E=0.60$ at 20 MeV and $\Delta E/E=0.27$ at 100 MeV. The energy spread resulted primarily from the finite thickness of the target and the size of tagging counters[4] required to produce a sufficiently intense photon beam. New high duty factor, high electron intensity accelerators now coming into service will make it possible to reduce the problem previously encountered.

A positron annihilation tagged photon method has been reported by Fultz et al.[6] but with a beam geometry that differs significantly from that used for measurements described here. In the Fultz system, one of the photons is detected in a plastic detector wrapped around the positron beam pipe located

ahead of the annihilation target. This system has the disadvantage that photons in the backward tagging counter have low energies (.26 to .51 MeV) and must be detected in a high background of other induced gamma rays in this energy region, while the other photon is nearly forward in the laboratory system and consequently is badly contaminated with bremsstrahlung photons (e.g., the total bremsstrahlung-to-annihilation photon ratio in the forward direction is $\sim$180 at 20 MeV).

A method is described here for obtaining the absolute photon detection efficiency and the angular and energy response functions of the Goddard Space Flight Center (GSFC) digitized spark chamber balloon borne telescope using the NBS positron annihilation-in-flight facility. The technique utilizes the two coincident photons that are produced from the annihilation of energetic positrons.

In the center-of-mass system the two annihilation photons are emitted back to back with equal energids. However, in the laboratory system the energies of the photons depends on the angle between the incident positron beam and the photons. In the method described here, one of the two annihilation photons, with an energy of $\sim$ 7 MeV, is detected at a fixed angle of 20° with respect to the incident positron beam. The detection of this photon signals the presence of, or "tags", the other annihilation photon which is used for the calibration measurement and which has an energy equal to the positron energy minus 7 MeV.

This paper reports the results of measurements of the absolute detection efficiency, and the angular and energy resolution of the GSFC gamma-ray telescope at 15.1 and 31.1 MeV. Following a brief description of the instrument, the details of the calibration beam configuration and tagging electronics are presented and measurements of the tagging efficiency are discussed. The experimental technique used to reduce the observed tagged counting rate to absolute efficiency, and the methods used to determine angular and energy resolution are presented. Finally, the observed data are compared with Monte Carlo calculations for the instrument.

2. INSTRUMENT DESCRIPTION

The detector is a digitized spark chamber gamma-ray telescope designed to study celestial gamma rays in the region of energy from 10 to 70 MeV. Prior to the calibration measurements described here, the instrument was flown twice using large ($8.7 \times 10^5 m^3$) balloons to study the diffuse gamma-ray emission from the galactic center region. A preliminary report on these results, together with a description of the instrument and a discussion of the data analysis including calibration information has already been published[7,8]. Only a brief discussion of the instrument is included here to assist in understanding the calibration measurements.

A schematic representation of the detector is shown in fig. 1. Two assemblies of spark chamber modules are separated by a central scintillator plane of thickness 0.63 cm. Each module has an active area of 50 cm x 50 cm and consists of two orthogonal wire grids each with 400 wires that are attached to a glass-bonded mica support frame. The electrical circuit of every wire includes a magnetic core memory, and these cores together with associated readout electronics are an integral part of each module.

The upper assembly contains 16 modules spaced by 1.44 cm and interleaved with 15 aluminum plates of thickness 0.0183 cm, while the lower assembly contains 4 modules and 3 aluminum plates with a spacing of 5.66 cm. The stack is encased in a thin aluminum pressure vessel filled with spark gas (99% neon and 1% ethane) at approximately one atmosphere. A thin window separates the bottom of the stack from a Cerenkov counter housed in a separate sealed volume along with system control and data-handling electronics.

The upper portion of the detector is covered by a plastic scintillator dome averaging 2 cm in thickness. Its purpose is to inhibit triggering of the instrument from charged cosmic radiation. In the upper atmosphere where this instrument

is designed to operate, the charged particle intensity is $\sim 10^4$ times the intensity of gamma rays within the energy range of the detector. This requires that the anticoincidence dome have a high efficiency to prevent the charged particles from seriously increasing the instrument dead time.

A gamma ray that enters the instrument may convert to a positron-electron pair in one of the aluminum plates in the upper assembly. When one or both of these particles propagate through the remaining telescope, a coincidence signal between the scintillator and Cerenkov counters triggers a high voltage pulse to the wire planes of each grid, provided that a veto signal from the anticoincidence dome is not present. Sparking between orthogonal wire planes occurs along the residual ion paths left by the particles, and the current pulses of the spark set the magnetic cores at the orthogonal coordinates in each module traversed by the particles. All of the chamber's 16,000 cores then are scanned and reset sequentially by the readout electronics. The addresses of set cores are encoded into the data stream, together with other ancillary information. The readout and high voltage pulser recycle time produces a dead time of approximately 450 msec per event during which further triggers of the instrument are inhibited.

The solid angle of the instrument is restricted by dividing the scintillator and Cerenkov planes into a 3 x 3 array of independent equal tiles. Signals from corresponding vertical pairs are required by the coincidence circuit. Further, the Cerenkov counter is used to discriminate against upward-moving events.

The spark locations for each event, together with a schematic overlay of the detector elements are plotted on microfilm under computer control. Event pictures are scanned to select only those with two particle tracks issuing from a vertex that is located within the spark chamber assembly above the scintillator

plane. In this way, an unambiguous selection of pair production events is made; and Compton scattering events, nuclear interactions in the module frames, and interactions in the pressure vessel are eliminated. After the gamma ray converts to charged particles, the aluminum plates serve as a scattering medium. For the selected events, analysis is completed by estimating the energy of each secondary particle using multiple scattering theory. The energy of the incident gamma ray then is determined and the direction of incidence is found by forming an energy-weighted bisector of the vertex in each projected view.

3. EXPERIMENTAL MEASUREMENTS

3.1 Beam Configuration

Fig. 2 shows the layout of the calibration beam and gamma-ray detector. This arrangement is similar to one used in an experiment already reported[9] and further details can be found there. The NBS linear accelerator is capable of producing a positron beam of energies up to 60 MeV. The beam was pulsed at a rate of 360 Hertz with a pulse width of 3.5 μsec. Average currents of up to 5 nA can be obtained, but in practice the beam was restricted to currents of approximately 0.1 nA to prevent pulse pileup in the various detectors. The beam was focused by a quadrupole pair (not shown in fig. 2) to maximize the number of photons produced in the forward direction.

A five position target ladder permits a variety of target foils to be selected remotely. Since the annihilation cross section is proportional to the atomic number Z of the target material while the bremsstrahlung cross section varies as Z^2, it is advantageous to select a low-Z material for the target. One position in the ladder contained a Be foil 44.8 mg/cm^2 thick which was the primary target used for calibration measurements discussed here. A thinner foil 9.4 mg/cm^2 thick was mounted into a second position in the ladder

to study the effect of multiple scattering in the target foil on the tagging efficiency. A third position in the ladder contained a Ta foil whose thickness was selected to produce the same bremsstrahlung intensity as the 44.8 mg/cm^2 Be foil. Comparison of count rates with the Be and Ta foils was useful in verifying the background due to bremsstrahlung. The remaining two positions of the target ladder were 1.27 cm and 2.54 cm diameter holes in 0.64 cm brass that were used for beam alignment and focusing.

Positrons which did not annihilate in the target were magnetically deflected through 90° into a shielded beam dump that consisted of an aluminum block. The integrated output of an electrometer connected to the beam dump was used to monitor the beam current. A parallel plate ionization chamber and a NaI(Tl) counter were also built into the dump system to monitor positron currents and to aid in initial setup of the beam.

Energetic positrons produce gamma rays primarily either by means of the bremsstrahlung process $e^+ + e^- \rightarrow e^+ + e^- + \gamma$ or from annihilation $e^+ + e^- \rightarrow 2\gamma$. For positron annihilation, the incident positron and photons are co-planar and the photon energy K is related to the positron total energy E and momentum P by

$$K = \frac{m}{1-[P/(E+m)]\cos\theta} \tag{1}$$

where m is the electron rest energy and θ is the angle of emission with respect to the beam. The observation of a photon in a cone of half angle $\Delta\theta_1$ at θ_1 implies that the second photon will occur in a cone $\Delta\theta_2$ at θ_2 given by (see reference 9)

$$\tan\theta_2 = \frac{m\sin\theta_1}{P\cos\Delta\theta_1 - E\cos\theta_1} \tag{2}$$

$$\tan\Delta\theta_2 = \frac{m\sin\Delta\theta_1}{E\cos\Delta\theta_1 - P\cos\theta_1}. \tag{3}$$

The beam defining collimator shown in fig. 2 consists of a lead slab 15.2 cm in thickness located 99 cm from the target. One of the two photons (the tagging photon) was observed at a fixed angle of 20° with respect to the beam, and the aperture wall defined a cone angle of 0.85° for this photon. As a consequence of this fixed angle and eqs. (2) and (3), the second photon had to be observed at an angle that depends upon the positron beam energy. To facilitate different energies, holes whose diameters and angles were determined by eqs. (2) and (3) were drilled in the collimator slab. Table 1 summarizes geometry for a variety of energies. Holes not in use were plugged with brass cylinders.

The tagging photon, at a fixed angle of 20°, varied in energy from 5.5 to 7.4 MeV over the range of positron energies for which the collimator geometry was designed. The tagging photon was detected by a NaI(Tl) crystal 12.7 cm diameter by 12.7 cm thick, surrounded by lead and borated polyethylene shielding. At the position of this crystal, the collimator defined a beam of 5.2 cm diameter which was small compared to the diameter of the detector. With the 44.8 mg/cm^2 Be annihilation target, the integrated bremsstrahlung intensity was comparable to the annihilation photon intensity in the tagging counter. The bremsstrahlung component is a continuous spectrum that varies roughly as K^{-1} up to the beam energy and consequently it can be nearly eliminated by using a differential discriminator to select only those events with energies around the annihilation peak. (See reference 9 for details.)

The higher energy tagged photon (photon 1 in fig. 2) traversed the collimator and entered the gamma-ray telescope which was situated approximately 8.5 m from the target. At this distance, the beam was 7.2 cm in diameter at 31 MeV and 13.4 cm in diameter at 15 MeV; dimensions which were small compared to the aperture of the detector. Provisions were included to translate the telescope remotely in the two orthogonal directions normal to the beam axis so that local variations in sensitivity within the instrument could be studied or averaged during calibration measurements. Also, the instrument could be tilted with respect to the beam to examine effects of zenith angle on the sensitivity and energy and angular resolution functions of the detector.

Among the photons that entered the instrument in the more forward direction with respect to the beam axis, the majority (90 to 95% depending on the range of angles and energies in table 1) were due to the bremsstrahlung background. (The charged particle backgrounds were rejected by the instrument anticoincidence scintillator dome.) Those photons observed in coincidence with the photons in the tagging detector, however, were due to the positron annihilation process and were the events used in this calibration. The energy dispersion of the annihilation photon beam was determined by the collimator geometry and was nominally 3%.

A condition on the intensity of the beam was set by limiting the event rate so that the probability of more than one pair image was small in any readout of the instrument. If ε is the probability of a pair conversion within the detector volume ($\varepsilon \sim 5\%$ at 30 MeV), N is the total number of gamma rays per beam burst, τ is the image retention time of the detector ($\tau \sim 1$ usec) and δ is the burst duration ($\delta = 3.5$ usec), the upper limit condition on the intensity set by the instrument characteristics is

$$N\varepsilon\tau/\delta \lesssim 0.1 \qquad (4)$$

For the values indicated above, eq. (4) implies a gated intensity of $N \lesssim 7$

photons per burst. Annihilation events were only about 5% of the total flux, however, and so the limiting annihilation rate was $N_a \sim 0.3$ per burst which was somewhat less restrictive than the limit required to avoid pile-up effects from the total intensity (annihilation plus bremsstrahlung) in the tagging counter. In practice, beam current was limited to ~ 0.12 nA with a corresponding annihilation intensity of $N_a \sim 0.02$ photons per burst.

Not all of the tagging events were accompanied by coincidence photons in the more forward aperture. Multiple scattering of the positrons in the annihilation foil altered the incident beam directions by rms angular intervals which were comparable with opening angles subtended by the holes in the collimator wall. Thus, the precise angular and energy correlation implied by eqs. (2) and (3) were blurred resulting in a reduction in the incidence counting rate. The spatial extent, position and focusing of the incident positron beam also influenced the coincidence rate due to the geometric constraints of the collimator. In practice, the beam could be tuned to provide a beam cross section centered on the target with a diameter of $\sim$1.5 cm. Finally, bremsstrahlung could produce photons in the tagging detector in the same energy interval as the annihilation photons. Because of these effects, it was necessary to measure the fraction of the tagging detector counts that were accompanied by photons in the forward aperture, hereafter called the tagging efficiency. For this purpose a second NaI(Tl) detector diameter 25.4 cm and thickness 25.4 cm long was moved into the forward beam ahead of the gamma ray telescope in fig. 2. Hayward et al.[9] have described this instrument and the manner in which coincidence measurements between the two NaI(Tl) counters were made. In summary, the counting rate of the larger crystal, gated by the tagging counter and the beam gate, was determined and corrected for the small fraction (1.1%) of the events that did not interact in the NaI(Tl), or because of the response function of the detector, produced signals too small to be counted (10.1%).

The ratio of the corrected coincidence rate to the singles rate in the tagging counter was then the tagging efficiency. Typically, this value ranged from 20 to 40%, depending on the energy, aperture geometry, and alignment and focus of the beam. During calibration measurements of the gamma-ray telescope, the tagging efficiency was observed before and after each measurement session, and their values are summarized in table 2.

3.2 Electronics

Fig. 3 shows a schematic of the electronics employed in the calibration measurements. The upper dotted area describes the logic of the gamma ray telescope showing how the nine scintillator and Cerenkov counters, as described earlier, combined to form a trigger signal provided no signal was present in the anticoincidence dome and when the readout electronics was not actively processing an earlier event. Such a signal signified a neutral event (γ-ray) had interacted to produce charged secondaries (e^+, e^-) in the pair-production plates interleaving the spark chamber modules above the scintillator plane (See fig. 1). In order to include the additional requirements of a signal in the tagging detector and a beam gate, the anticoincidence scintillator dome signal line was broken and routed out of the instrument to a coincidence module whose other input was derived as shown schematically in the lower dotted box of fig. 3.

4. DATA ANALYSIS AND RESULTS.

Calibration measurements were made on five separate occasions. During each session, the spark event data were recorded on magnetic tape using the hard line connection shown in fig. 3. In addition, the gated tagging detector counts ($T \cdot G$) and the instrument trigger counts ($\bar{A} \cdot B \cdot C \cdot T \cdot G \cdot \bar{I}$) along with other secondary data including the beam dump counting rate, the beam current, and

the instrument anticoincidence dome rate were all recorded for each measurement interval. As noted earlier, tagging efficiencies were observed before and after each session. Furthermore, periodic checks of the beam focus were made using the beam-defining aperture in the ladder. The background due to bremsstrahlung was verified to be negligible through the use of the Ta target, and the effects of accidental coincidence were found to be unimportant by introducing long delays in one leg of the coincidence network.

The spark chamber event data were analyzed in the same manner as flight data[7,8]. In this procedure, source tapes were used to make computer-generated plots of each orthogonal view of the spark chamber assembly. The events were scanned by a trained observer to select those that clearly shows two secondary charged particles that originate at a vertex that was located below the top deck. This signature unambiguously identified that the $\gamma \rightarrow e^+ + e^-$ interaction occurred in the spark chamber volume. Some of the actual pair production events might have been rejected by the rigid selection criteria; however, the observed instrument sensitivity naturally included the selection efficiency. Each accepted event was "structured"[7,8] on an interactive computer display terminal. In this step, spark coordinates of each secondary electron were identified in both orthogonal views. Finally, the energy of the electron-positron pair was evaluated using multiple scattering theory, and the direction of the incident gamma ray was determined with respect to the chamber coordinates using an energy-weighted bisector of the two electrons.

Table 2 summarizes the calibration data used to measure the efficiency of the telescope at 31.1 and 15.1 MeV. As described above, the product of the tagging efficiency and the tagging detector counts represents the number of gamma rays from two photon annihilations in the beam target wich are incident on the telescope. Of that total, only a small fraction interact in the telescope and cause a trigger to occur, and still smaller fraction produce acceptable events

that meet scanning selection criteria. The instrument's efficiency then was determined from the ratio of accepted events to the product of tagging counts, tagging efficiency, and live-time fraction. The live-time fraction is determined by

$$L = 1-p(1-r\tau)\ \frac{n}{T} \tag{5}$$

with an uncertainty

$$\sigma_L \cong p(1-r\tau)\ \frac{\sqrt{n}}{T} \tag{6}$$

Here p is the readout time of the telescope (450 msec), r is the counting rate in the A-dome ($r \cong 2500$ cps during calibration), τ is the anticoincidence pulse width (1.0 μsec), and n is the total number of detector counts in time T.

It is evident from table 2 that the majority of the sessions were devoted to 31.1 MeV at vertical incidence where the technique was developed. However, the times devoted to each catagory of energy and direction are roughly equal. Observations that were suspect as a result of poor tuning or high current with resulting pile-up in the tagging counter have been eliminated from the results of table 2. The uncertainties expressed in this table are one standard deviation estimates based on counting statistics only. Other uncertainties, for example, drifts in the beam focus and cross sectional area could produce systematic biases as well as additional random error. For these reasons, the average value for 31.1 MeV at 0.0 degrees incidence is a simple average rather than a weighted mean. It should be noted, however, that the individual measurements are in statistical agreement.

The results summarized in table 2 are plotted in fig. 4, together with curves calculated using a Monte Carlo program tailored to this spark chamber telescope. Here, the ordinate is the product of the efficiency and the active area (2500 cm^2) of the instrument. The actual calculated efficiency values are reduced by a factor of 1.3 in order to normalize them to the calibration

data. This factor is not unexpected in view of several simplifying approximations that tend to overestimate efficiency in the Monte Carlo approach. Some of these approximations include chamber edge effects where escaping particles can trigger the anticoincidence system, the simple threshold for signals in the scintillators and Cerenkov counters, and the event selection effects mentioned above wherein actual scanning some events may be rejected when their vertex is not clearly defined in the event pictures. The analytic approach, when anchored with observed data as in fig. 4, provides a useful means of extending the information on sensitivity to other angles and energies.

Measures of energy and angle resolving ability of the instrument are obtained for the same set of events by comparing the observed quantities with the known energy and direction of the calibration beam. Fig. 5a summarizes the projected-view rms angular resolution as a function of energy compared with the functions predicted by the Monte Carlo program. The full three dimensional angular uncertainty is larger than the values of fig. 5a by $\sqrt{2}$. Fig. 5b shows the energy resolution obtained for the 31.1 MeV data. This distribution is skewed towards low energies since energy is essentially inversely related to the angular deviation due to multiple scattering which is a symmetric distribution. The width of this distribution is 36% of the mean value. The number of events at 15.1 MeV are too few to provide a meaningful histogram, but they too have a width $\sim$ 35% of the mean of 15 MeV. Monte Carlo simulations suggest $\Delta E/E \sim 35\%$ for all energies from 15 to 70 MeV. Above 70 MeV, deviations of particle trajectories due to multiple scattering are dominated by uncertainties in track coordiantes due to the quantized nature of wire grid spark chamber coordinate measuring capabilities.

5. SUMMARY

A tagged photon beam produced from in-flight annihilation of positrons that was developed at NBS provided a nearly monoenergetic beam of photons useful for calibrating detectors in the energy range from 10 to 50 MeV at the NBS linear

accelerator. Measurements of the GSFC balloon-borne gamma-ray telescope properties at 15 and 31 MeV furnished data for verifying and normalizing the Monte Carlo analysis of the telescope performance.

The authors wish to thank Dr. Evans Hayward and Dr. Donald Kniffen for stimulating discussions and assistance during measurements. In addition, they are grateful to Dr. Hayward for making available the large NaI(Tl) counter used to measure tagging efficiency. Further, they wish to thank Dr. Daniel Morris for assistance in the event data selection and analysis.

REFERENCE

1. G.W. Clark, G.P. Garmire, and W.L. Kraushaar, 12th Intern. Cosmic-ray conf. papers, vol. 1 (Hobart, 1971) p. 91.

2. R.C. Hartman, C.E. Fichtel, D.A. Kniffen, and D.J. Thompson, 13th Intern. Cosmic-ray conf. papers, vol. 4 (Denver, 1973) p. 2733.

3. C.E. Fichtel, R.C. Hartman, D.A. Kniffen, D.J. Thompson, G.F. Bignami, H. Ögelman, M.E. Özel, and T. Tümer, Astrophys. J. 198 (1975) 163.

4. G.F. Bignami, J. Paul, E. Pfeffermann, B.N. Swanenburg, A. Scheepmaker, W.H. Voges, and R.D. Wills, Nucl. Instr. and Meth. 108 (1973) 257.

5. H. Christ, F. Peters, G.F. Bignami, J.J. Burger, W. Hermsen, J.A. Paul E. Pfeffermann, B.G. Taylor, W.H. Voges, and R.D. Wills, Nucl. Instr. and Meth. 116 (1974) 477.

6. S.C. Fultz, R.L. Bramblett, J.T. Caldwell, and N.A. Kerr, Phys. Rev. 127 (1962) 1273.

7. D.A. Kniffen, D.L. Bertsch, D.J. Morris, R.A.R. Palmeira, and K.R. Rao, Proc. 12th ESLAB Symp. (Frascati, 1977) p. 117.

8. D.A. Kniffen, D.L. Bertsch, D.J. Morris, R.A.R. Palmeira, and K.R. Rao, Astrophys. J. 225 (1978) 591.

9. Evans Hayward, William R. Dodge, Bryan, H. Patrick, Nucl. Instr. and Meth. 159 (1979) 289.

TABLE 1

Annihilation Energies And Angular Relationships

POSITRON	PHOTON 1			PHOTON 2		
E (MeV)	K_1 (MeV)	θ_1 (Deg)	$\Delta\theta_1$ (Deg)	K_2 (MeV)	θ_2 (deg)	$\Delta\theta_2$ (deg)
55.00	48.01	3.02	0.13	7.41	20.0	0.86
37.61	31.10	4.42	0.19	7.00	20.00	0.86
31.24	24.97	5.32	0.23	6.76	20.00	0.86
26.72	20.67	6.22	0.27	6.54	20.00	0.86
20.74	15.10	8.01	0.35	6.14	20.00	0.86
14.38	9.39	11.53	0.50	5.49	20.00	0.86

TABLE 2

SUMMARY OF EFFICIENCY MEASUREMENTS

RUN NUMBER	TOTAL EXPOSURE TIME (MIN.)	PHOTON ENERGY (MEV)	INCIDENCE ANGLE (DEGREES)	TAGGING COUNTER		GAMMA RAY TELESCOPE			
				COUNTS	EFFICIENCY (%)	TOTAL TRIGGERS	ACCEPTED EVENTS*	LIVE-TIME (%)	EFFICIENCY † (%)
2	30	31.1	0.0	8,980	18.2 ± 2.2	152	23.6	96.0 ± 0.3	1.50 ± 0.36
3	30	31.1	0.0	19,560	20.9 ± 1.3	357	60.4	90.8 ± 0.5	1.63 ± 0.23
4	168	31.1	0.0	72,870	30.8 ± 2.0	775	277.6	96.3 ± 0.1	1.28 ± 0.11
5a	80	31.1	0.0	29,410	17.7 ± 0.8	251	74	97.4 ± 0.1	1.46 ± 0.18
5b	363	31.1	20.0	125,700	17.7 ± 0.8	556	158.1	98.6 ± 0.1	0.721 ± 0.067
6	337	15.1	0.0	130,500	41.4 ± 1.6	341	20	99.0 ± 0.1	.037 ± .0084

† THE AVERAGE EFFICIENCY OF RUNS NUMBERED 2, 3, 4 & 5a IS 1.47 ± 0.16 PERCENT

* CORRECTED FOR SCANNING SELECTION EFFICIENCY

FIGURE CAPTIONS

Fig. 1. Schematic of the GSFC medium-energy digitized spark chamber gamma ray telescope.

Fig. 2. A plan view of the positron and annihilation photon beam geometry used for the gamma ray telescope calibration measurements. Detection of photon 2 at a fixed angle of 20° served to tag the coincident photon 1 as the companion annihilation photon. The collimator allows angle θ, to be changed to accommodate geometries appropriate for a range of energies (see table 1).

Fig. 3. Block diagram of the electronics logic and data system used for the tagged calibration measurements. The upper dashed box represents the coincidence and event processing electronics integral to the GSFC gamma ray telescope, altered as noted, to incorporate the tagging logic derived as shown in the lower dashed box.

Fig. 4. The observed area (2500 cm^2) x efficiency of the gamma ray telescope. The uncertainties are one standard deviation based on counting statistics alone. Solid curves are calculated Monte Carlo results divided by 1.3 to normalize them to observed data (see text for details).

Fig. 5. Observed resolution functions for the gamma ray telescope. Fig. 5a shows data and calculated (Monte Carlo) results, given by the solid curve, for the angular resolution in a projected plane. Full three dimensional angular uncertainty is larger by a factor $\sqrt{2}$. In fig. 5b the observed event energies determined by multiple scattering measurements are shown together with the overall mean of 29.6 MeV given by the dotted line. The spread of this distribution is $\approx$35%.

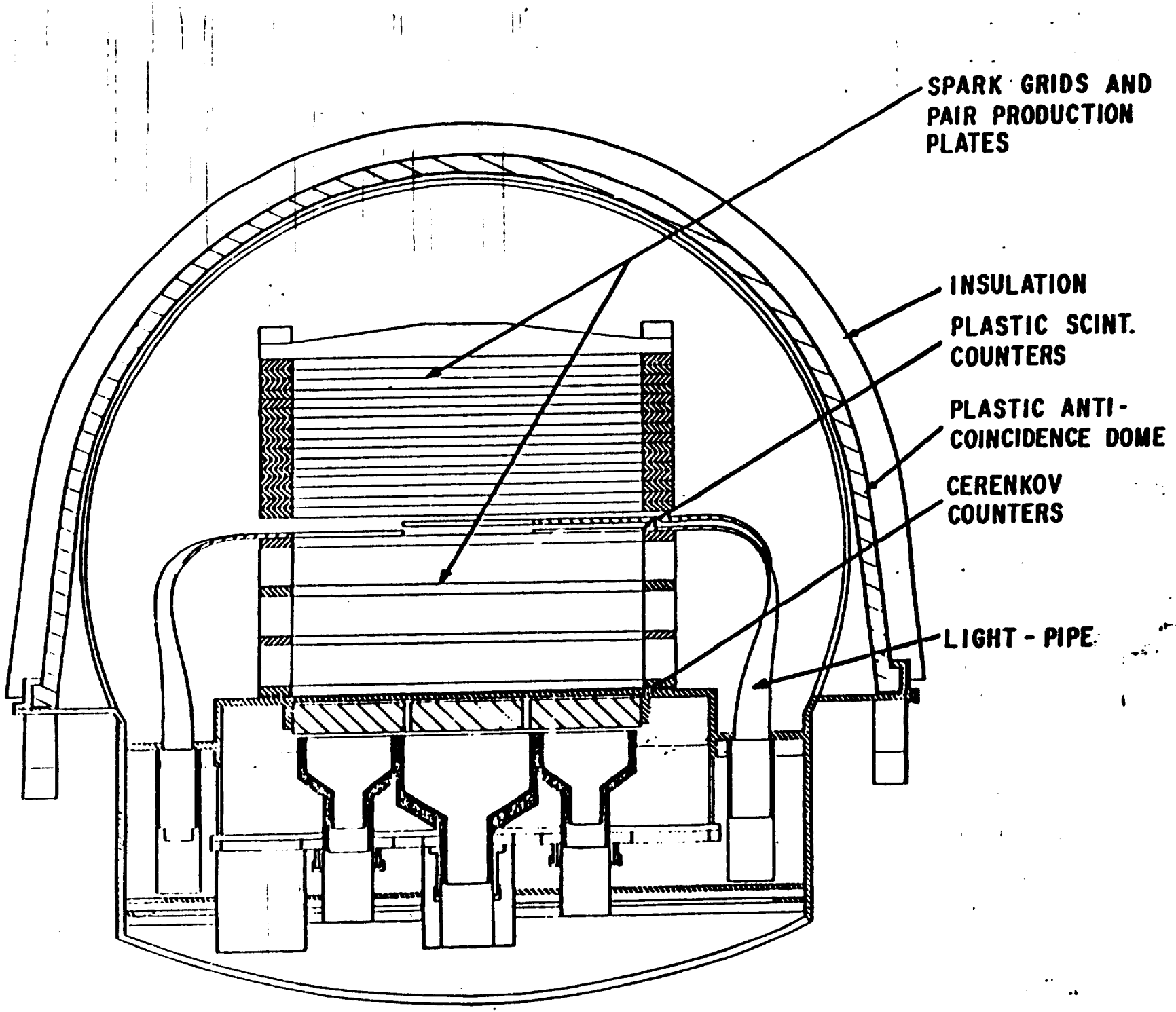
SPARK GRIDS AND
PAIR PRODUCTION
PLATES
INSULATION
PLASTIC SCINT.
COUNTERS
PLASTIC ANTI-
COINCIDENCE DOME
CERENKOV
COUNTERS
LIGHT - PIPE

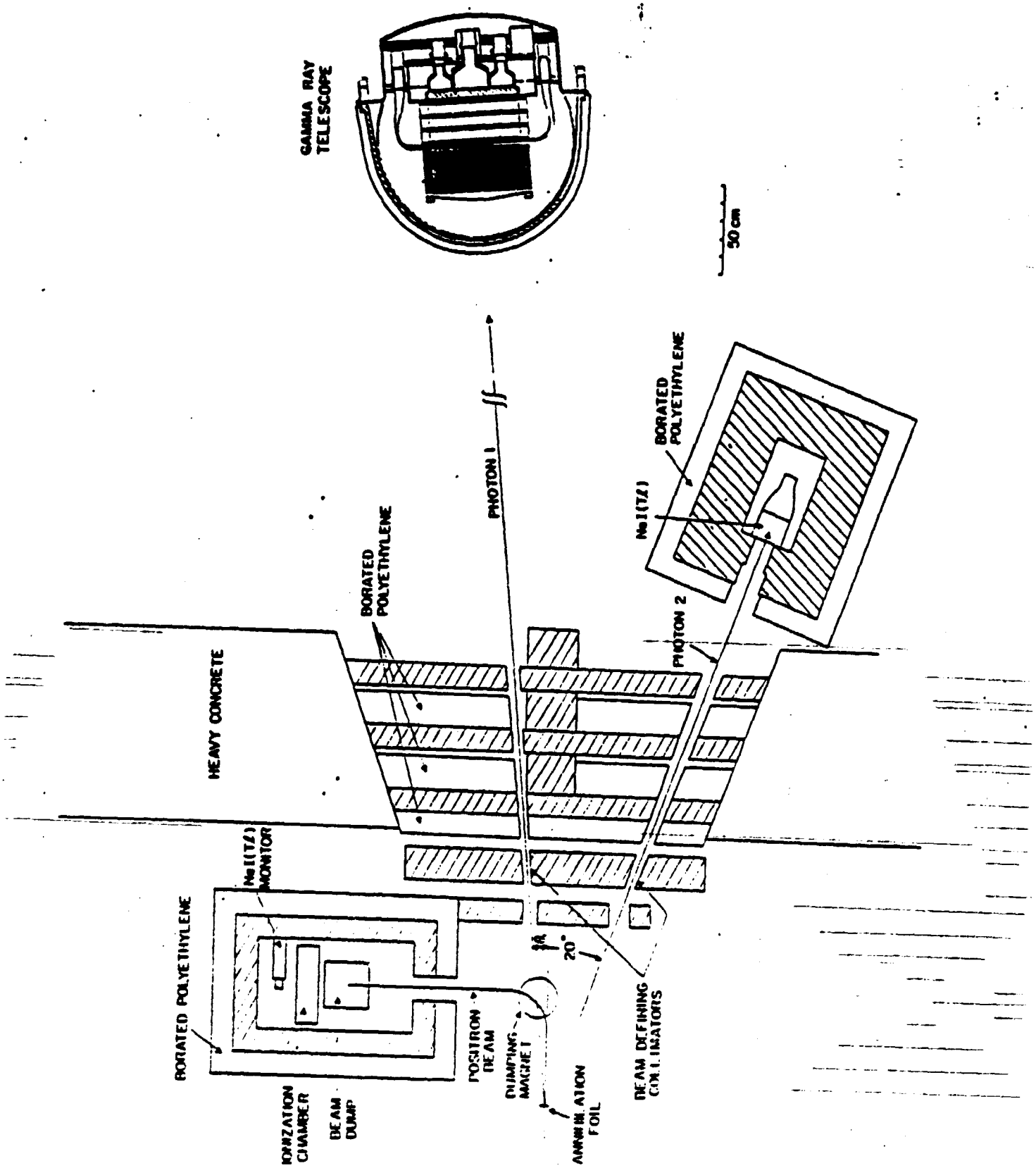

ORIGINAL PAGE IS
OF POOR QUALITY

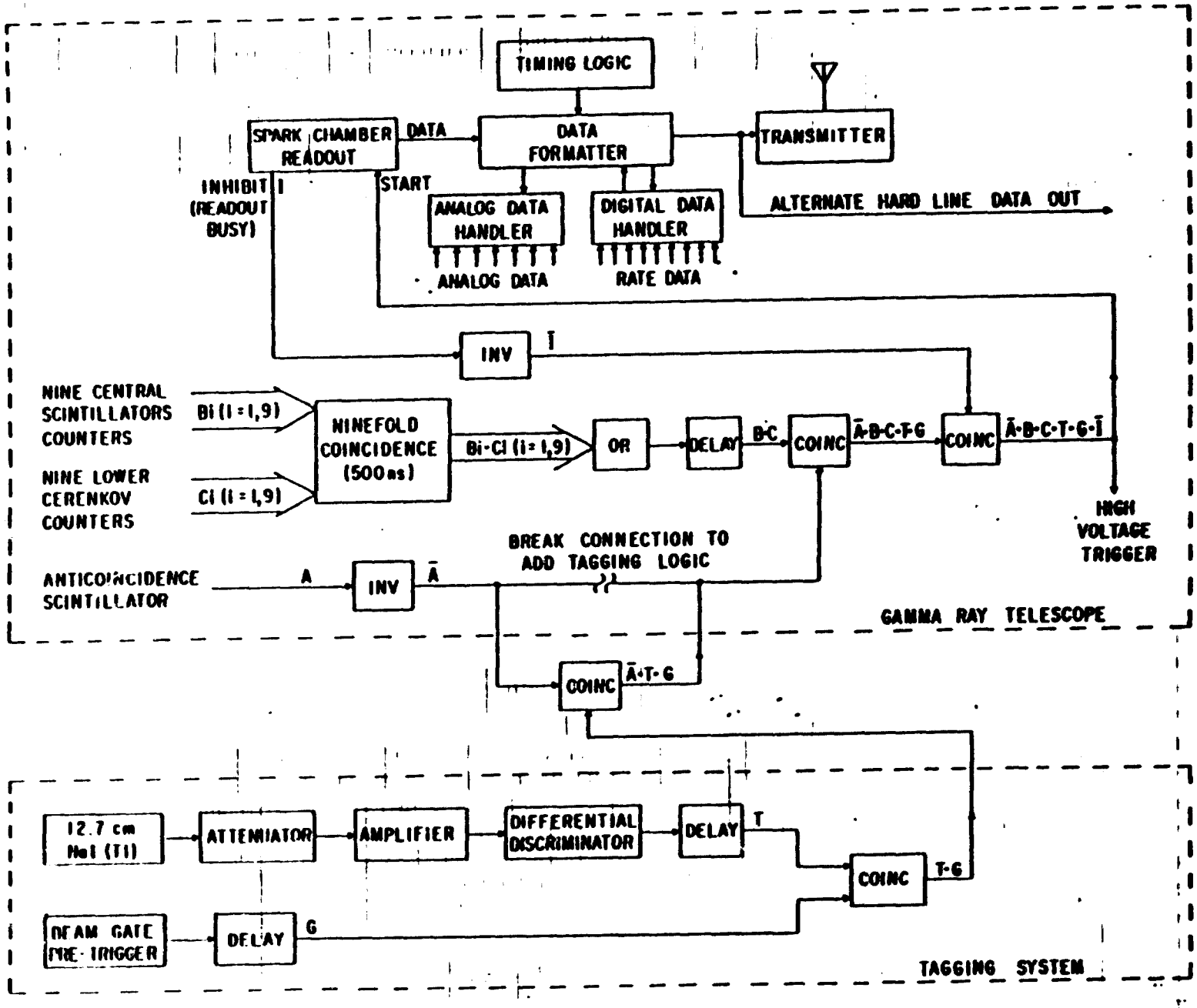
TIMING LOGIC
SPARK CHAMBER READOUT
DATA
DATA FORMATTER
TRANSMITTER
INHIBIT (READOUT BUSY)
I
START
ANALOG DATA HANDLER
DIGITAL DATA HANDLER
ALTERNATE HARD LINE DATA OUT
ANALOG DATA
RATE DATA
INV
Ī
NINE CENTRAL SCINTILLATORS COUNTERS
Bi (i = 1,9)
NINE LOWER CERENKOV COUNTERS
Ci (i = 1,9)
NINEFOLD COINCIDENCE (500 ns)
Bi·Ci (i = 1,9)
OR
DELAY
B·C
COINC
Ā·B·C·T·G
COINC
Ā·B·C·T·G·Ī
HIGH VOLTAGE TRIGGER
BREAK CONNECTION TO ADD TAGGING LOGIC
ANTICOINCIDENCE SCINTILLATOR
A
INV
Ā
GAMMA RAY TELESCOPE
COINC
Ā·T·G
12.7 cm NaI (Tl)
ATTENUATOR
AMPLIFIER
DIFFERENTIAL DISCRIMINATOR
DELAY
T
COINC
T·G
BEAM GATE PRE-TRIGGER
DELAY
G
TAGGING SYSTEM

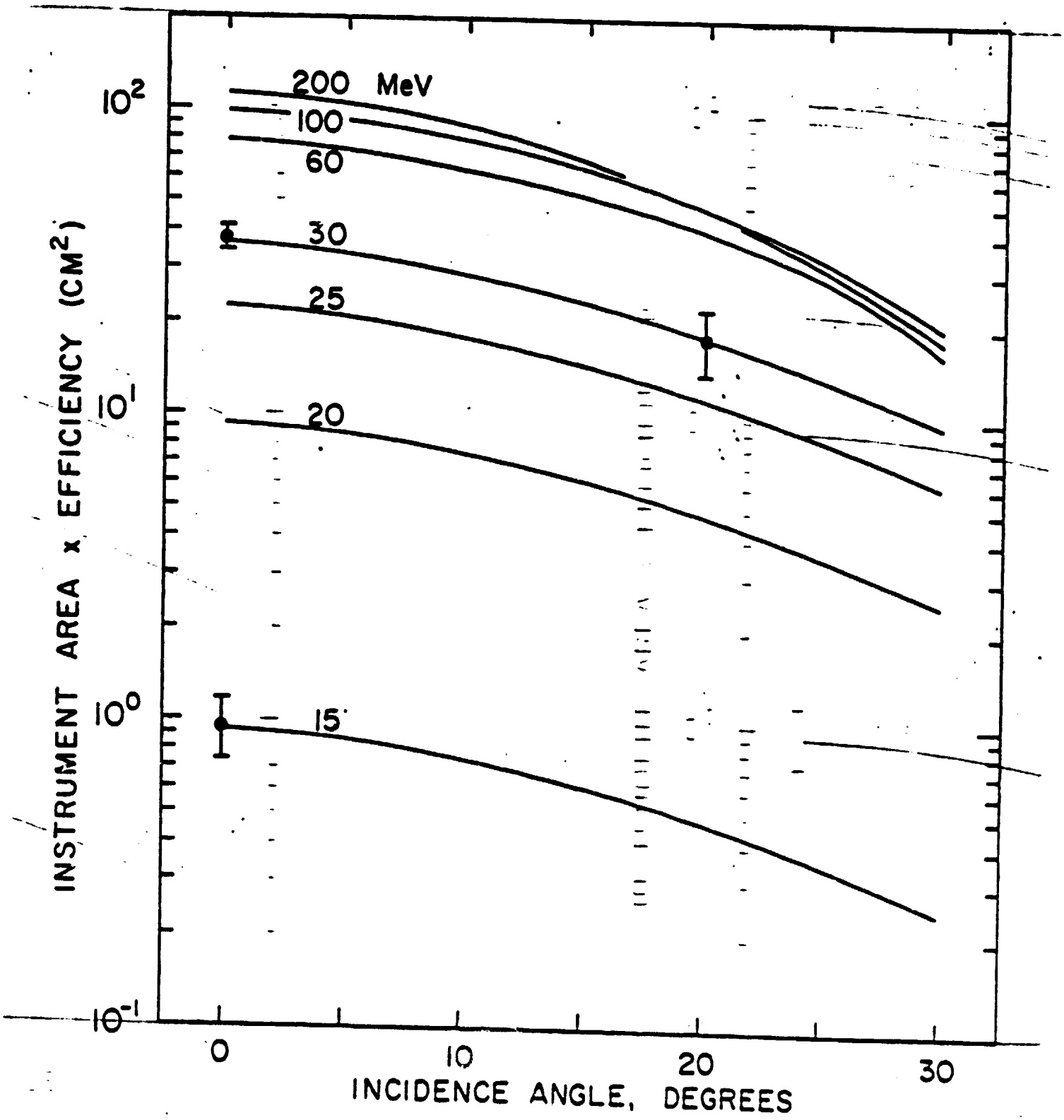
200 MeV
100
60
30
25
20
15
10^2
10^1
10^0
10^{-1}
INSTRUMENT AREA x EFFICIENCY (CM^2)
0
10
20
30
INCIDENCE ANGLE, DEGREES

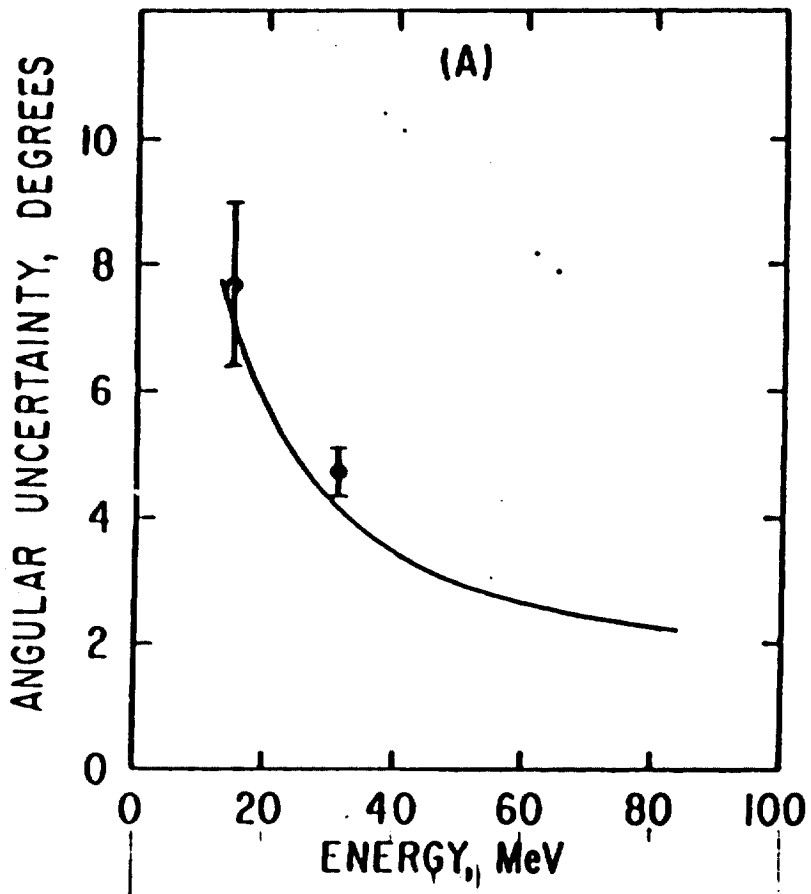

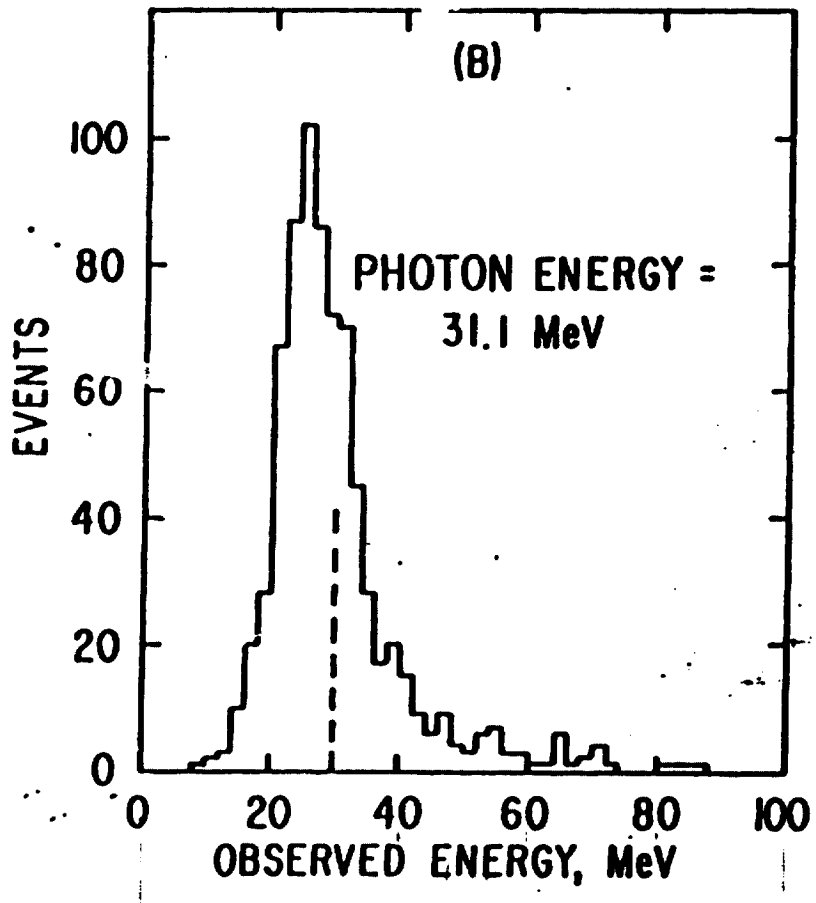

ORIGINAL PAGE IS
OF POOR QUALITY